Hadron production in hadron-nucleus and nucleus-nucleus collisions in the dual Monte Carlo multichain fragmentation model

J. Ranft*

Superconducting Super Collider Central Design Group, Lawrence Berkeley Laboratory, University of California, Berkeley, California 94720

(Received 2 October 1987)

Hadron production in hadron-nucleus and nucleus-nucleus collisions is studied by a Monte Carlo version of the dual multichain fragmentation model. The model takes into account leading-order corrections due to the secondary interactions of low-energy secondaries inside the target nucleus. An empirical formation time parameter is introduced and used to decide which secondaries interact again inside the target. Data for the multiparticle production in proton-nucleus and oxygen-nucleus interactions at 200 GeV/nucleon from different experiments are well described by the model and consistent with a formation-time parameter of $\tau c = 2 \pm 1$ fm.

I. INTRODUCTION

In this paper high-energy nucleon-nucleus and nucleus-nucleus collisions will be studied within one and the same model.

High-energy collisions of heavy ions offer the possibility to discover experimentally the quark-gluon plasma,[1] a new state of matter. Experimental studies using nuclei accelerated up to energies of 200 GeV per nucleon started in 1986 at the CERN Super Proton Synchrotron. First experimental results have become available.[2,3]

Experiments on inelastic hadron-nucleus collisions have been performed for many years. There exist numerous models which try to describe and understand the data, see Ref. 4, where the experimental and phenomenological situation is reviewed.

In order to understand which signatures of heavy-ion collisions point to the formation of a quark-gluon plasma, we should study such collisions within conventional models of hadron physics for soft-particle production. Scattering events predicted by such conventional models are the background against which the effects of the quark-gluon plasma have to be found.

The Monte Carlo version of the dual multistring fragmentation model has been applied successfully to hadron-hadron collisions,[5,6] hadron-nucleus collisions,[7,8] and nucleus-nucleus collisions.[9,10] The same models have also been studied using different techniques.[11-14]

In Sec. II the dual multistring fragmentation model for hadron-nucleus and nucleus-nucleus collisions will be defined. In Sec. III leading-order corrections to this model are introduced. These corrections concern secondary interactions of some of the low-energy hadrons created in the collisions inside the nucleus. The concept of a formation time[15] is used in order to decide under which conditions such secondary interactions are possible. In Sec. IV details about the Monte Carlo model are given and in Sec. V the model is compared to experimental data and discussed.

II. THE DUAL MONTE CARLO MULTICHAIN FRAGMENTATION MODEL

The dual Monte Carlo multichain fragmentation model has been applied before to hadron-nucleus collisions[7,8] and to nucleus-nucleus collisions.[9,10] These models correspond closely to models studied by other groups,[11,13,14] mainly with non-Monte Carlo methods.

Here we implement the model both for nucleon-nucleus and nucleus-nucleus collisions. In nucleon-nucleus and nucleus-nucleus collisions many elementary interactions occur. In Fig. 1 we give an example for a nucleon-nucleus collision. The collision is characterized by a total of n elementary collisions. In each elementary collision particles are produced via two multiparticle chains; therefore, the total number of chains is $2n$. In each inelastic nucleon-nucleus collision the projectile nucleus ($n_p = 1$) and $n_t = n$ target nucleons take part. The multiparticle chains have either valence quarks and diquarks at their ends or sea-quark–antiquark pairs. $n-1$ sea-quark pairs of the projectile nucleon are needed to form the chains. The elementary collisions can be classified as valence-valence and valence-sea collisions.

In nucleus-nucleus collisions the situation is quite similar. In Fig. 2 we give an example for the chain structure of a nucleus-nucleus collision. There are altogether n elementary collisions with n_p projectile and n_t target nucleons involved. For $n_p < n_t$ we have (i) $2n_p$ valence-valence chains $[q_p^v\text{-}(qq)_t^v]$ and $[(qq)_p^v\text{-}q_t^v]$, (ii) $2(n_t - n_p)$ valence-sea chains $[q_p^s\text{-}(qq)_t^v]$ and $(\bar{q}_p^s\text{-}q_t^s)$, and (iii) $2(n - n_t)$ sea-sea chains $(q_p^s\text{-}\bar{q}_t^s)$ and $(\bar{q}_p^s\text{-}q_t^s)$. The q^s, $\bar{q}^s$, q^v, and $(qq)^v$ stand here for sea quarks, sea antiquarks, valence quarks, and valence diquarks.

The average numbers of collisions n and participating nucleons n_p and n_t depend only weakly on the collision energy. However, at low collision energies the invariant masses of many sea-sea chains turn out to be below the masses of the mesons, which could be formed out of the quarks and antiquark at the end of the chains. The kine-

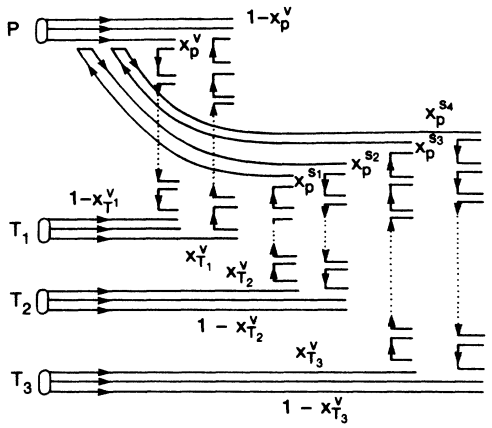

FIG. 1. Example of a triple-scattering diagram in a proton-nucleus interaction. P represents the incoming proton and T_1, T_2, and T_3 are three target nucleons taking part in the interaction. x^v and x^{si} are valence- and sea-quark momentum fractions.

matics at low collision energies forces the suppression of many sea-sea chains.

If the invariant masses of q-$\bar{q}$ chains are between the masses of the pseudoscalar mesons and vector mesons with the appropriate quark composition we replace the chains by the pseudoscalar mesons and correct the kinematics correspondingly. If the invariant mass of the chains is between the masses of the vector mesons m_v and $m_v+\Delta$ ($\Delta\approx 300$ MeV/c^2), we replace the chains by the vector mesons and correct the kinematics in such a way that energy and momentum conservation remain satisfied. In the case of quark-diquark chains we proceed similarly with the octet and decuplet baryons. Chains with masses below the masses of pseudoscalar mesons and octet baryons are suppressed and energy and momentum of the suppressed chains are given to the valence-

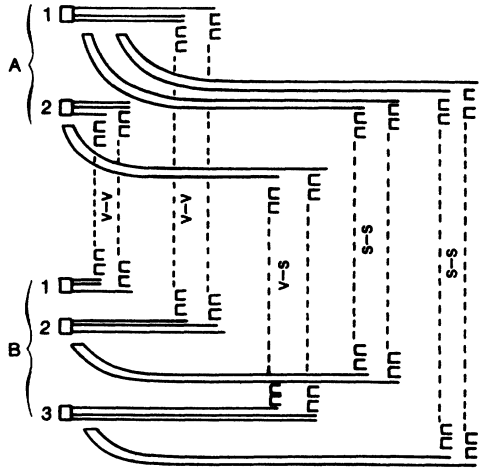

FIG. 2. Example of a nucleus-nucleus scattering process with $n=5$ interactions and $n_A=2$ contributing nucleons from the projectile nucleus A and $n_B=3$ contributing nucleons from the target nucleus B. This gives rise to four valence-valence chains, two valence-sea chains, and four sea-sea chains.

valence and valence-sea chains.

The distributions of the numbers n, n_A, and n_B in collisions of the nuclei A and B follow from Glauber theory. We follow here the formulation and Monte Carlo algorithms of Zadorozhnyi, Uzhinskii, and Shmakov.[14] The total inelastic collision cross section of the nuclei A and B is given as an integral over the impact parameter b:

$$\sigma_{AB}^{\text{inel}}=\int d^2b\left[1-\prod_{i=1}^{A}\prod_{j=1}^{B}(1-\sigma P_{ij})\right]\left[\prod_{i=1}^{A}\frac{T_A(\mathbf{s}_i)}{A}d^2s_i\right]\times\left[\prod_{j=1}^{B}\frac{T_B(\tau_j)}{B}d^2\tau_j\right]=\int d^2b\,\Gamma(\mathbf{b})\ . \tag{1}$$

A and B designate here also the number of nucleons in the nuclei A and B. The vectors $\mathbf{s}_i$ and τ_i give the positions of the nucleons i and j in the two nuclei. σP_{ij} is given by

$$\begin{aligned}\sigma P_{ij}&=\sigma P(\mathbf{b}-\mathbf{s}_i+\tau_i)\\&=\gamma(\mathbf{b}-\mathbf{s}_i+\tau_i)+\gamma^*(\mathbf{b}-\mathbf{s}_i+\tau_i)\\&\quad-\gamma(\mathbf{b}-\mathbf{s}_i+\tau_i)\gamma^*(\mathbf{b}-\mathbf{s}_i+\tau_i)\ ,\end{aligned} \tag{2}$$

where $\gamma(b)$ is the elastic N-N scattering amplitude as a function of the impact parameter b.

The expression for the total inelastic cross section can be written as a sum over cross sections with ν inelastic nucleon-nucleon interactions:

$$\sigma_{AB}^{\text{inel}}=\sum_{\nu=1}^{AB}\sigma_\nu \tag{3}$$

with

$$\sigma_\nu=\frac{(-\sigma)^\nu}{\nu!}\frac{d^\nu}{d\sigma^\nu}\int d^2b\left[\prod_{i=1}^{A}\prod_{j=1}^{B}(1-\sigma P_{ij})\right]\times\left[\prod_{i=1}^{A}\frac{T_A(\mathbf{s}_i)}{A}d^2s_i\right]\times\left[\prod_{j=1}^{B}\frac{T_B(\tau_j)}{B}d^2\tau_j\right]\ . \tag{4}$$

From this expression Zadorozhnyi, Uzhinskii, and Shmakov[14] work out the algorithm for sampling the events characterized by n, n_A, and n_B and by the individual nucleons between which the collisions occur.

In particular, for $\nu=1$ collision one obtains, from (4),

$$\sigma_1=\int d^2b\left[\sum_{i=1}^{A}\sum_{j=1}^{B}\sigma P_{ij}\prod_{\substack{k=1\\(k,l)\neq(i,j)}}^{A}\prod_{l=1}^{B}(1-\sigma P_{kl})\right]\times\left[\prod_{k=1}^{A}\frac{T_A(\mathbf{s}_k)}{A}d^2s_k\right]\left[\prod_{l=1}^{B}\frac{T_B(\tau_l)}{B}d^2\tau_l\right]\ . \tag{5}$$

For $\nu=2$ collisions one obtains terms where one nucleon of A interacts with two different nucleons of B, where one nucleon of B interacts with two different nucleons of A, and finally where two different nucleons of A interact with two different nucleons of B:

$$\sigma_2=\int d^2b\left[\frac{1}{2}\sum_{\substack{i,j=1\\ i\neq j}}^{A}\sum_{k=1}^{B}\sigma^2P_{ik}P_{jk}\prod_{\substack{l=1\\ (l,m)\neq(i,k),(j,k)}}^{A}\prod_{m=1}^{B}(1-\sigma P_{lm})+\frac{1}{2}\sum_{i=1}^{A}\sum_{\substack{j,k=1\\ j\neq k}}^{B}\sigma^2P_{ij}P_{ik}\prod_{\substack{l=1\\ (l,m)\neq(i,j),(i,k)}}^{A}\prod_{m=1}^{B}(1-\sigma P_{lm})\right.$$
$$\left.+\frac{1}{2}\sum_{\substack{i,j=1\\ i\neq j}}^{A}\sum_{\substack{k,l=1\\ k\neq l}}^{B}\sigma^2P_{ik}P_{jl}\prod_{\substack{m=1\\ (m,n)\neq(i,k),(j,l)}}^{A}\prod_{n=1}^{B}(1-\sigma P_{mn})\right]$$
$$\times\left[\prod_{i=1}^{A}\frac{T_A(\mathbf{s}_i)}{A}d^2s_i\right]\left[\prod_{j=1}^{B}\frac{T_B(\tau_j)}{B}d^2\tau_j\right]. \tag{6}$$

The contributions to any number ν of collisions can be constructed and envisaged in a graphical way as indicated in Fig. 3 for $\nu=1$ and 2.

In Fig. 4 we plot the number of participating projectile nucleons obtained from the Monte Carlo algorithm for collisions of oxygen and sulfur ions with different nuclei.

Central collisions can be defined as collisions where all nucleons of the projectile nucleus interact. (It is assumed that the projectile nucleus is lighter than the target nucleus $A_p < A_t$.) It is visible from Fig. 4 that a rather large fraction of all collisions is central, provided the target nuclei are heavy enough.

III. THE INTRANUCLEAR CASCADE CORRECTION

At energies well above 3–5 GeV per nucleon the dual multichain fragmentation model provides a picture of multiparticle production in hadron-nucleus and nucleus-nucleus collisions, which is superior to the intranuclear cascade model.[16] In contrast with this, at energies below 3–5 GeV the intranuclear cascade model provides a good description of inelastic nuclear collisions. At these energies the dual multichain fragmentation model is difficult to apply since most of the quark-antiquark and quark-diquark chains have masses below the masses of the hadrons with the same quark composition. Therefore, at these energies this model would mainly be determined by the particular way used to implement the kinematical suppression of the chains.

The physical picture, which explains the absence of the intranuclear cascade at high energies, is the concept of the formation zone.[15] Secondary hadrons in the collisions are not formed instantaneously. In their rest frame they need a certain time distributed exponentially[17] with the average τ, which we call the formation time, before they are present as complete hadronic states. Before this time we might understand them in the quark model as states consisting only out of valence quarks, without the full system of sea quarks, antiquarks, and gluons. These hadrons have a reduced probability for hadronic interactions inside the nucleus because of the absence of the soft components in the hadronic state.

In this picture it appears to be quite natural that most of the fast secondaries created in nuclear collisions have no possibility for secondary interactions inside the nucleus. Because of the relativistic time dilation they are created at positions where the secondary hadronic system is already outside the nucleus. This explains the absence of the intranuclear cascade at high energies.

The argument for the absence of secondary interactions inside the nucleus applies only to high-energy secondary hadrons, not to particles with low energies, which are created inside the target nucleus. This is also consistent with phenomenological observations. For secondary particles with rapidities below $y\approx 2$ in the tar-

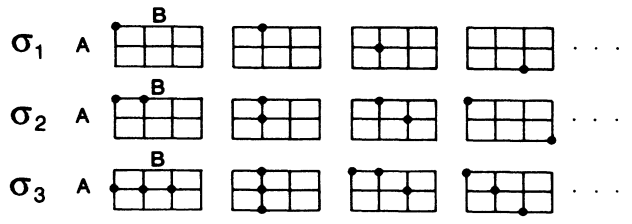

FIG. 3. Graphical representation of some of the contributions to the cross sections with $n=1$, 2, and 3 elementary scatterings. For $n=2$ and 3 there are contributions with multiple interactions of one target or projectile nucleon.

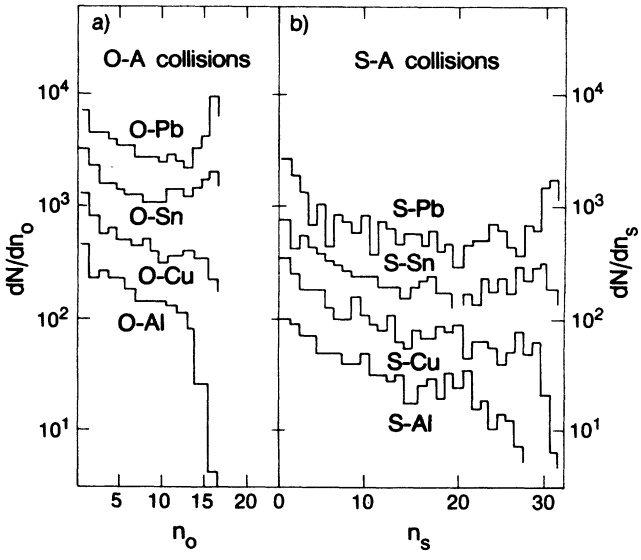

FIG. 4. Distribution in the number of projectile nucleons taking part in collisions of oxygen and sulfur ions with different nuclei. The peaks at $n_O=16$ and $n_S=32$ correspond to central collisions: (a) O-A collisions, (b) S-A collisions.

get rest frame the model predictions were found to be too low compared to the data in our previous[8] study of the dual multichain fragmentation model as applied to hadron-nucleus collisions. Starting from these qualitative and phenomenological arguments we propose here a leading-order correction to slow secondary particle production in asymmetric collisions ($A_p \ll A_t$) in the dual multichain fragmentation model. We introduce an empirical parameter τ, which we call the hadronic formation time.

In the dual Monte Carlo multichain fragmentation model as formulated above we know for each collision event the positions $\mathbf{s}_i$ and τ_j of all interacting nucleons in the rest frames of the two nuclei as well as the impact parameter b of the collision. We know also which nucleons are engaged in the elementary collisions. In the model we determine the energies and momenta of the secondary particles created. This information gives us the full space-time history of the collisions. In any particular Lorentz frame we can follow the trajectories of the secondaries created in space and time. We choose, in particular, the target rest frame, which seems to be the natural frame to describe asymmetric collisions of projectile nucleons or light projectile nuclei with heavy target nuclei. In this frame we can trace the trajectory of each secondary hadron with mass m_1, energy E_1, momentum $\mathbf{p}$ and Lorentz parameters $\gamma = E/mc^2$ and $\boldsymbol{\beta}\gamma = \mathbf{p}/mc$:

$$\mathbf{x} = \mathbf{x}_0 + \dot{\mathbf{x}}t, \quad \dot{\mathbf{x}} = \boldsymbol{\beta}c \ . \tag{7}$$

We assume that the secondary hadron starts to interact hadronically in its rest frame after the formation time τ or after the time $\tau_t = \gamma\tau$ in the target rest frame. Assuming a target nucleus with fixed radius R we get the time t_{12} when the secondary particle leaves the target nucleus from

$$(\mathbf{x}_0 + \dot{\mathbf{x}}t)^2 = R^2 \tag{8}$$

or

$$t_R = -\frac{\mathbf{x}_0 \cdot \dot{\mathbf{x}}}{\dot{\mathbf{x}}^2} + \left[\left(\frac{\mathbf{x}_0 \cdot \dot{\mathbf{x}}}{\dot{\mathbf{x}}^2} \right)^2 - \frac{\mathbf{x}_0^2 - \mathbf{R}^2}{\dot{\mathbf{x}}^2} \right]^{1/2} . \tag{9}$$

A particular secondary particle has the chance to interact again inside the nucleus for

$$\tau_t < t_R \ . \tag{10}$$

Since we are only interested in the leading-order corrections to the multistring fragmentation model we consider such secondary collisions only for hadrons produced in the primary collision. We do not go on to follow the intranuclear cascade for all low-energy hadrons created in turn in the secondary collisions, and so on.

It has to be recognized that the scheme proposed is in no way Lorentz invariant. The conditions for secondary interactions differ if we go into different Lorentz frames, for instance, into the projectile rest frame. In this situation we apply the scheme only to highly asymmetric collisions such as hadron-nucleus collisions or nucleus-nucleus collisions with light projectiles as studied in present experiments.[2,3] We leave for the future the generalization of this scheme to collisions of heavy projectiles and targets and the construction of a full intranuclear cascade for the soft hadrons.

IV. THE MONTE CARLO MODEL

The first step in the generation of each event is the sampling of the positions of all nucleons in the two colliding nuclei, the sampling of the impact parameter, and, using the Glauber theory, sampling the number of elementary collisions n and participating nucleons n_p and n_t. All this is described in Sec. III and in the paper of Zadorozhnyi, Uzhinskii, and Shmakov.[14] In an earlier version of the model[9] we did use the distribution[13] for sampling the number of collisions. This formulation is equivalent to the one used here. However, the method[14] allows a more efficient Monte Carlo sampling and provides at the same time a detailed model for the nucleons of the projectile at certain positions hitting definite target nucleons also at known positions.

From the n, n_p, and n_t the chain structure of the event is fixed and we sample next the flavors and momentum fractions x of the valence quarks, diquarks, and sea-quark–antiquark pairs at the end of the chains. It is to be noted, that the x values of the valence and sea quarks to be used in a model for soft-particle production are not constrained by the data from deep-inelastic lepton-hadron interactions or by other hard hadronic processes. This model cannot be derived from perturbative QCD. Nevertheless, one finds phenomenologically these distributions to look quite similar to the familiar structure functions. We use for valence quarks the distribution

$$q^v(x) = \frac{N^v}{\sqrt{x}}(1-x)^2 \ , \tag{11}$$

and, for sea quarks and antiquarks,

$$q^s(x) = \frac{N^s}{x}(1-x)^6 \ . \tag{12}$$

More important than the powers in $(1-x)$ in these distributions is the small x behavior, which is obtained by dual-Regge arguments.[18] What we really need are the exclusive quark distributions for all valence quarks and diquarks and the k sea-quark–antiquark pairs at the end of the chains originating from a given nucleon:

$$f(x_q^v, x_{qq}^v, x_{q_1}^s, x_{\bar{q}_1}^s, \ldots, x_{q_k}^s, x_{\bar{q}_k}^s) = q_q^v(x_q^v) q_{qq}^v(x_{qq}^v) \prod_{i=1}^{k} q^s(x_{q_i}^s) q^s(x_{\bar{q}_i}^s) \delta \left[1 - x_q^v - x_{qq}^v - \sum_{i=1}^{k} (x_{q_i}^s + x_{\bar{q}_i}^s) \right] . \tag{13}$$

We satisfy this distribution by sampling first the x values of all valence and sea quarks from the distributions (11) and (12) and giving at the end to the diquark the x value

$$x_{qq}^{v}=1-x_{q}^{v}-\sum_{i=1}^{k}(x_{q_i}^{s}+x_{\bar{q}_i}^{s}) . \tag{14}$$

In our rejection method we have to reject all events where the sum over all x values becomes larger than 1. Therefore, the input distributions (11) and (12) are modified by the sampling procedure. The output distributions will, for instance, depend on the number of collisions. We give also to each multiparticle chain a transverse momentum sampled from the distributions

$$\frac{dn}{p_\perp dp_\perp}=Ne^{-BE_\perp}, \quad E_\perp=\sqrt{p_\perp^2+m^2} , \tag{15}$$

with average transverse momenta in the order of 0.4 GeV/c. The exponential distribution in the transverse energy gives for hadrons automatically the mass dependence of the transverse-momentum distribution and the average transverse momenta as found in experiment. For our model this distribution is mainly significant for these strings, which at low invariant mass degenerate into single hadrons. For these hadrons Eq. (15) is the only source of transverse momentum. For hadrons resulting from string decay the transverse momentum obtained from the string decay is more important. Therefore, the model as a whole is rather insensitive to the shape of (15) and the corresponding average chain transverse momentum. The transverse momenta of the two chains which belong to each elementary collision are chosen to be opposite to each other.

The next step in the Monte Carlo calculations is the fragmentation of all chains with masses above the masses of the vector mesons and decuplet baryons. These chains are fragmented using the chain decay code BAMJET,[19] which was originally constructed to describe quark-antiquark chains found in hadronic electron-positron events. BAMJET fragments quark-antiquark, quark-diquark, and diquark-antidiquark chains into pseudoscalar and vector mesons and octet and decuplet baryons. Subsequently, all hadronic resonances decay; this is sampled using the code DECAY.[20]

Besides the primary elementary collisions of the dual chain fragmentation model we have also to sample the events corresponding to secondary interactions of hadrons with nucleons inside the nucleus as described in Sec. III. These collisions are at rather low energies, often below 1 GeV. Therefore, it is not practical to sample them using again the multichain fragmentation model. We use instead the code HADRIN,[21] which samples inelastic hadron-hadron collisions at energies below 5 GeV in good agreement with experiment. HADRIN samples inelastic collisions via quasi-two-body reactions and subsequent resonance decay. In our present, not fully developed, intranuclear cascade we do not sample the formation zones from the exponential distribution. In doing so we would need to sample some of these secondary collisions at energies above the range where HADRIN is applicable. Without this approximation we expect the formation-zone parameter to become slightly larger than the ones found here.

The complete hadron-nucleus or nucleus-nucleus events are checked by the conservation laws for energy, momentum, and additive quantum numbers such as charge, strangeness, and baryon number. All those conservation laws are satisfied by the individual events sampled.

All distributions presented in this paper are obtained by sampling between 1000 and 2000 events. Depending on the reaction, between 2 and 20 min CPU time on a IBM 3090 computer are needed to create these events.

V. RESULTS AND COMPARISON WITH DATA

The model without the intranuclear cascade correction was already compared to data from oxygen-lead collisions at 200 GeV (Ref. 10). Here we want to continue these comparisons and to study the influence of the formation time parameter τ. The τ parameter will be determined from comparison with experiments.

The global effect of the formation time correction can be seen from Fig. 5 where we plot the multiplicities of secondary protons, π^+, charged particles, and all secondaries in p-Pb and O-Pb collisions as function of τc. The multiplicity of secondary protons (and the multiplicity of neutrons, which behaves quite similarly) shows the strongest variation with τ. Most of the additional particles produced by the intranuclear cascade corrections are nucleons. This is consistent with the expectations.

We compare different calculated distributions in

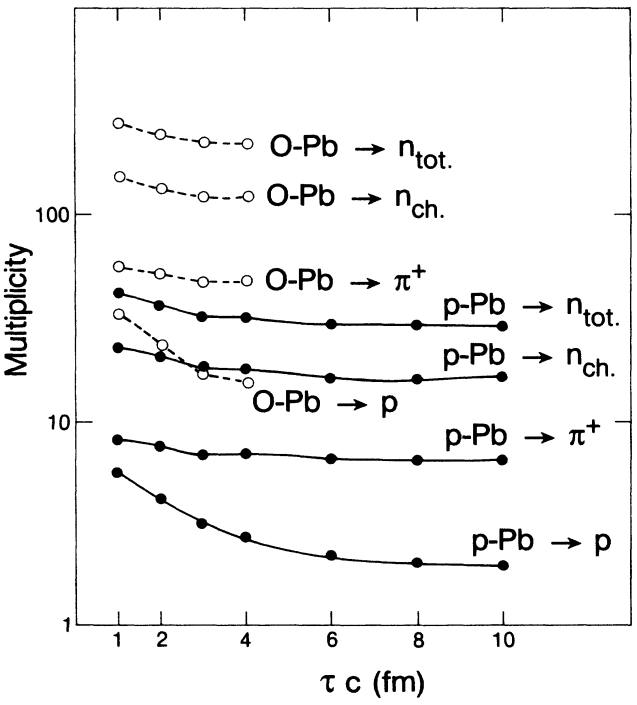

FIG. 5. Multiplicities of secondary protons, π^+, charged hadrons, and all produced particles in p-Pb and O-Pb collisions as function of the formation-time parameter τc.

nucleon-nucleus collisions with experimental data in order to determine the formation-time parameter τ.

(i) In Ref. 8 rapidity distributions and rapidity ratios

$$R^{A}(y)=\frac{dN^{p-A}}{dy}\Big/\frac{dN^{p-p}}{dy} \tag{16}$$

are calculated in the dual multichain fragmentation model and compared to data in p-Xe collisions at 200 GeV (Ref. 22). A disagreement is found at low rapidities in the target rest frame. Above rapidities $y\approx 2$ the agreement of the model and the measured rapidity distributions and rapidity ratios was rather good. At rapidities below $y\approx 2$ the measured rapidity ratios were bigger than the calculated ones.

In Fig. 6 we compare this rapidity ratio calculated with different τc parameters again with the data.[22] The rapidity ratio calculated in Ref. 8 corresponds in the present model to the limit $\tau\to\infty$; practically, as seen from the multiplicities in Fig. 6 this means $\tau c=6-10$ fm. Now we find a good agreement down to laboratory rapidities of $y=0$. The optimum formation-time parameter in this comparison is

$$\tau c=1-2 \text{ fm} \quad \text{(rapidity ratios in } p\text{-Xe collisions)} . \tag{17}$$

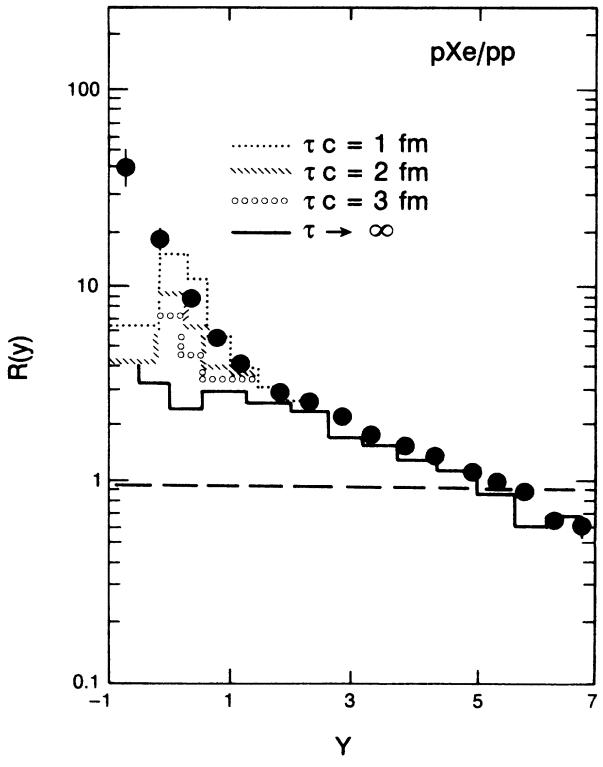

FIG. 6. Rapidity ratios $R(y)=[dN/dy(p\text{-Xe})]/[dN/dy(p\text{-p})]$ for all charged particles at proton energies in the laboratory frame $p_{\text{lab}}=200$ GeV/c. The Monte Carlo results represented by histograms are compared to data from Ref. 22. The lowest histogram corresponding to $\tau\to\infty$ was already calculated in Ref. 8.

(ii) The transverse-energy distribution $d\sigma/dE_{\perp}$ was measured by the HELIOS (NA34) Collaboration at the CERN Super Proton Synchrotron[23] in proton-lead collisions. The data are taken in the pseudorapidity range $0.6\le\eta\le 2.4$. In this rapidity range the intranuclear cas-

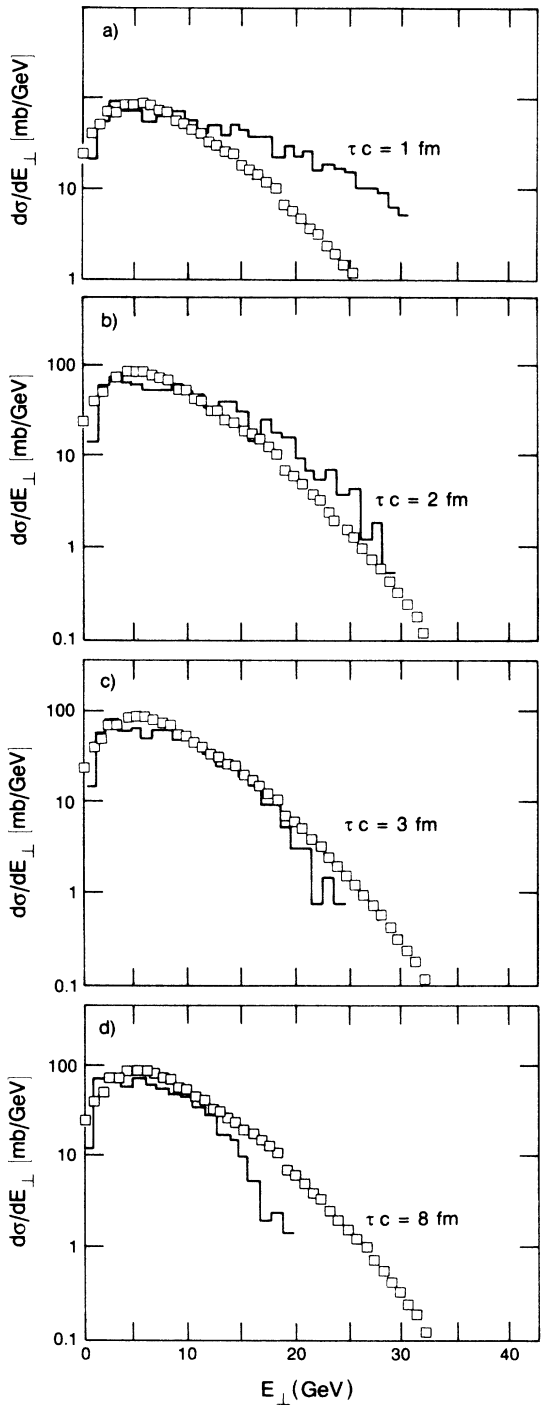

FIG. 7. Transverse-energy distributions $d\sigma/dE_{\perp}$ for protons interacting on Pb nuclei. The calculations given by histograms are compared to data (points) from the HELIOS Collaboration (Ref. 23) measured in the pseudorapidity range $0.6\le\eta\le 2.4$. The calculation was done with different formation-time parameters τc: (a) $\tau c=1$ fm, (b) $\tau c=2$ fm, (c) $\tau c=3$ fm, (d) $\tau c=8$ fm.

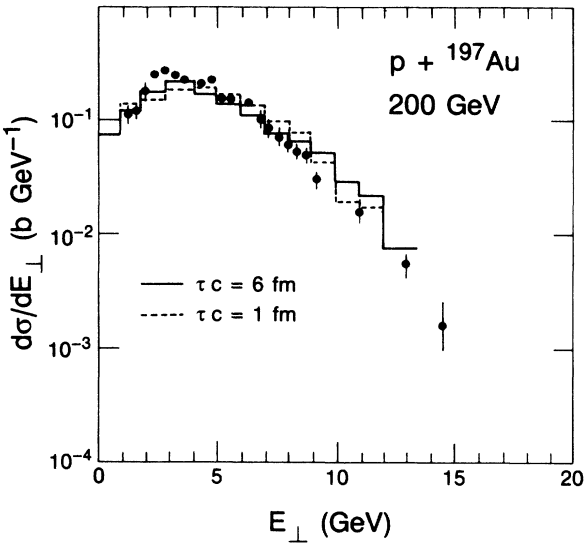

FIG. 8. Transverse-energy distributions $d\sigma/dE_\perp$ for protons interacting on Au nuclei. The calculations given by histograms are compared to data (points) from the NA35 Collaboration[2] measured in the rapidity range $2.2 \leq \eta \leq 3.8$. The Monte Carlo results are presented for two different values of the formation-time parameter τ.

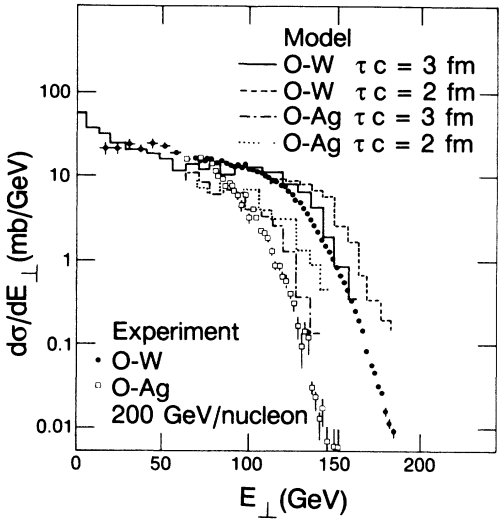

FIG. 10. Transverse-energy distributions in O-Ag and O-W collisions with 200 GeV per nucleon. The results of the Monte Carlo calculation (histograms) are compared with experimental data (points) of the HELIOS Collaboration (Ref. 3). The model results are given for two values of the formation-time parameter τ.

cade corrections to the model are significant. In Fig. 7 we compare the transverse-energy distribution for different τ values with the data.[23] We find the best agreement for

$$\tau c = 2-3 \text{ fm} \quad (d\sigma/dE_\perp \text{ in } p\text{-Pb collisions}) . \tag{18}$$

(iii) Transverse-energy distributions in p-Au collisions were also measured by the NA35 Collaboration at the CERN Super Proton Synchrotron.[2] This experiment is sensitive for laboratory rapidities $2.2 \leq y \leq 3.8$. In this rapidity range we do not expect significant changes of the

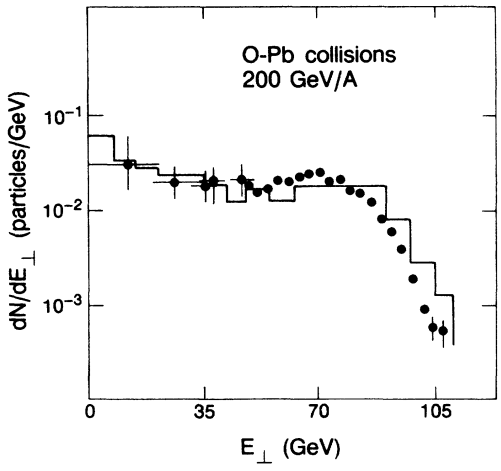

FIG. 9. The transverse-energy distribution in O-Pb collisions with 200 GeV per nucleon. The results of the model (histogram) are compared with experimental data (points) from the NA35 Collaboration (Ref. 2).

$d\sigma/dE_\perp$ distributions with the τ parameter. In Fig. 8 we find indeed a good agreement of the model for $\tau c = 1$ fm as well as for $\tau c = 6$ fm with the data. It is not possible to determine the τ parameter from this experiment. The model agrees well with the data.

We conclude from these three comparisons that the model agrees well with data in nucleon-nucleus collisions. The optimum formation-time parameter is around $\tau c = 2$ fm.

Next we compare the model with transverse-energy distributions measured in oxygen-nucleus collisions at energies of 200 GeV per nucleon. In Fig. 9 we compare the model with O-Pb data from the NA35 Collaboration at the CERN Super Proton Synchrotron.[2] The data are again for the rapidity range $2.2 \leq y \leq 3.8$. In this rapidity region the model is practically independent on the formation time parameter τ. We find a good agreement of the model with the data.

The transverse-energy distribution in oxygen-silver and oxygen-tungsten collisions was measured by the HELIOS Collaboration.[3] This experiment is sensitive to pseudorapidities in the range $-0.1 \leq \eta \leq 2.9$. In this range the results of the model depend strongly on the formation time parameter τ. In Fig. 10 we compare the data[3] with the model calculations for $\tau c = 2$ and 3 fm. The calculation with $\tau c = 3$ fm agrees better with the data than the one with $\tau c = 2$ fm. This is slightly inconsistent with what we found above from proton-nucleus collisions. We find in both comparisons with oxygen-nucleus collisions presented in Figs. 9 and 10 that the model overestimates somewhat the cross sections at the largest $E_\perp$ values. In order to be more specific as to what is calculated we specify the following. For π and K mesons we add for each individual particle $E_\perp = \sqrt{m^2 + p_\perp^2}$ to the $E_\perp$ histograms. For protons and neutrons, which are not identified in the ex-

periments, only the transverse momenta $p_\perp$ are added to the $E_\perp$ histograms. Changes in the model predictions could result from changes in the scattering amplitudes entering in (2) or the nuclear density distributions in (1) and (4). In spite of these small disagreements we tend to conclude that the model agrees remarkably well with the experimental data available so far for nucleus-nucleus collisions. From this agreement it can be concluded that these data cannot be interpreted as evidence for new physics such as the quark-gluon plasma.

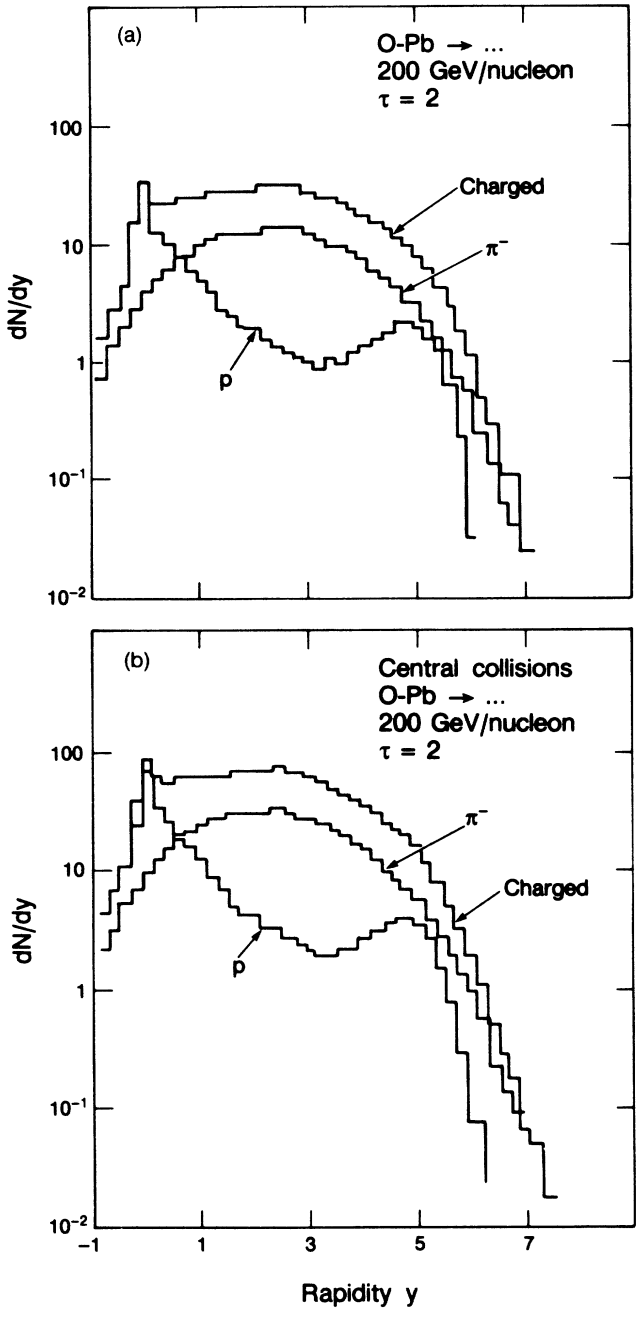

FIG. 11. Rapidity distributions of secondary protons, π^- mesons, and all charged particles in O-Pb collisions with 200 GeV per nucleon as calculated by the model: (a) normal collisions, (b) central collisions only.

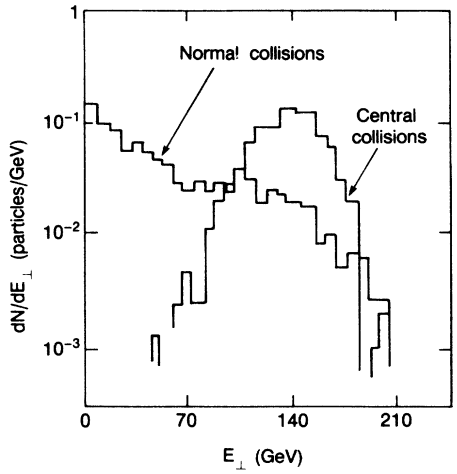

FIG. 12. Transverse-energy distributions as calculated for normal and central collisions with a formation-time parameter $\tau c = 2$ fm for all secondaries in the rapidity range $-0.1 \leq \eta \leq 2.9$ for O-Pb collisions.

After these comparisons we present some calculated distributions which help us to understand the model. In Fig. 11(a) rapidity distributions are given for hadrons produced in oxygen-lead collisions. The distributions refer to all charged particles, secondary protons, and π^- mesons. The secondary proton distribution (and the very similar secondary neutron distribution) shows a remarkable shape. There are two maxima. One maximum at low rapidities corresponds to the fragmentation products of the target nucleus; the second at large rapidity corresponds to the projectile nucleons, which were involved in

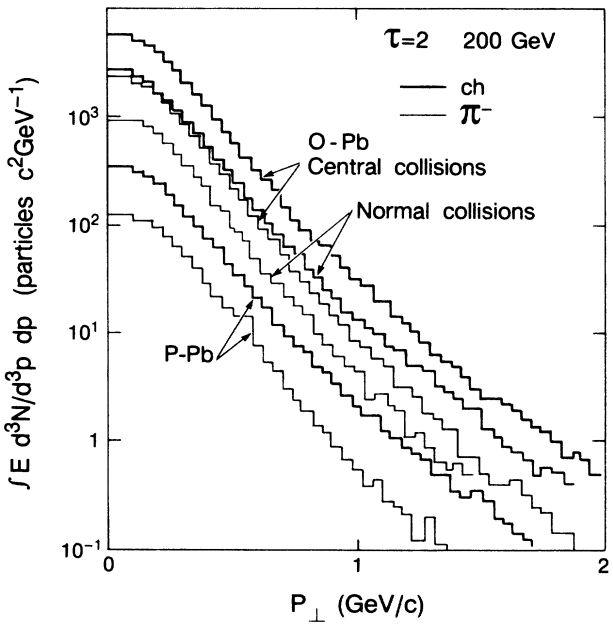

FIG. 13. Transverse-momentum distributions of all charged particles and π^- mesons as calculated for p-Pb and normal and central O-Pb collisions.

the inelastic collisions. Such distributions of secondary nucleons have been used to discuss the concept of the nuclear stopping power.[24,25] The dual multistring fragmentation model makes detailed predictions for this.

Central collisions are defined as collisions where all projectile nucleons interact $n_p = A_p$. In Fig. 11(b) the rapidity distributions resulting from central collisions are presented. Except for the higher overall production no striking qualitative changes are visible as compared to the normal collisions.

In Fig. 12 we compare transverse-energy distributions obtained in central collisions with the ones in normal collisions. It can be concluded from this comparison, that the tail of the normal $E_\perp$ distribution results from central collisions. Central collisions offer the best opportunities to find evidence for the formation of the quark-gluon plasma. Events with maximum $E_\perp$ are therefore the most interesting ones to look for the effects of the quark-gluon plasma.

Finally we present in Fig. 13 transverse-momentum distributions obtained in the model for p-Pb and for normal and central O-Pb collisions. All $p_\perp$ distributions look rather similar. It should be stressed that the model does not incorporate hard-hadronic collisions; therefore, we expect the model distribution to remain below the data above some sufficiently high transverse momentum. The $p_\perp$ distribution is mainly the result of the $p_\perp$ distribution used in the chain fragmentation model.[19] Slightly below $p_\perp = 1$ GeV/c the slope of the $p_\perp$ distribution of all charged particles changes. This flattening of the $p_\perp$ distribution is due to the secondary protons, which have a larger average $p_\perp$ than pions. This effect is more significant in nucleus-nucleus collisions because of the increased fraction of secondary nucleons in these collisions as compared to hadron-nucleus collisions.

ACKNOWLEDGMENTS

Part of this study was done during a stay at CERN, Geneva. It was completed at the Superconducting Super Collider (SSC) central design group. I would like to thank Dr. K. Goebel at CERN and Professor M. Tigner at SSC for their hospitality. Acknowledgments are due to Dr. H.-J. Möhring and Dr. S. Ritter, who did collaborate in the first steps of this investigation, and to Dr. S. Yu. Shmakov for discussions and for a FORTRAN program sampling the distribution from Ref. 14.

*Permanent address: Sektion Physik, Karl-Marx-Universität, Leipzig, German Democratic Republic.

[1]E. V. Shuryak, Phys. Rep. **61**, 71 (1980); *Quark Matter Formation and Heavy Ion Collisions,* proceedings of the Workshop, Bielefeld, Germany, 1982, edited by M. Jacob and H. Satz (World Scientific, Singapore, 1982); R. Hagedorn, Riv. Nuovo Cimento **6**, 1 (1984).

[2]NA35 Collaboration, A. Bamberger *et al.*, Phys. Lett. B **184**, 271 (1987).

[3]HELIOS Collaboration, Y. Sirois, *et al.*, in the Proceedings of the XXII Rencontre de Moriond, 1987 (to be published).

[4]M. A. Faessler, Ann. Phys. (N.Y.) **137**, 44 (1981); S. Fredriksson, G. Eilam, G. Berlad, and L. Bergström, Phys. Rep. **144**, 187 (1987); N. N. Nikolaev, Usp. Fiz. Nauk **134**, 369 (1981) [Sov. Phys. Usp. **24**, 531 (1981)].

[5]J. Ranft and S. Ritter, Z. Phys. C **27**, 413 (1985); J. Ranft, *ibid.* **33**, 517 (1987).

[6]P. Aurenche, F. W. Bopp, and J. Ranft, Z. Phys. C **23**, 67 (1984); Phys. Rev. D **33**, 1867 (1986).

[7]J. Ranft and S. Ritter, Z. Phys. C **20**, 347 (1983).

[8]J. Ranft and S. Ritter, Z. Phys. C **27**, 569 (1985).

[9]H. J. Möhring, J. Ranft, and S. Ritter, Z. Phys. C **27**, 419 (1985).

[10]J. Ranft, Phys. Lett. B **188**, 379 (1987).

[11]A. Capella and J. Tran Thanh Van, Phys. Lett. **93B**, 146 (1980); Nucl. Phys. **A461**, 501c (1987).

[12]A. B. Kaidalov and K. A. Ter-Martirosyan, Yad. Fiz. **39**, 1545 (1984) [Sov. J. Nucl. Phys. **39**, 979 (1984)]; A. B. Kaidalov, K. A. Ter-Martirosyan, and Yu. M. Shabelskii, *ibid.* **43**, 1282 (1986) [*ibid.* **43**, 822 (1986)].

[13]A. Capella, C. Pajares, and A. V. Ramallo, Nucl. Phys. **B241**, 75 (1984).

[14]A. M. Zadorozhnyi, W. W. Uzhinskii, and S. Yu. Shmakov, Dubna Report No. P2-86-361, 1986 (unpublished).

[15]L. Landau and I. Pomeranchuk, Dok. Akad. Nauk SSSR **92**, 535 (1953); **92**, 734 (1953); E. L. Feinberg, Zh. Eksp. Teor. Fiz. **50**, 202 (1966) [Sov. Phys. JETP **23**, 132 (1966)].

[16]H. W. Bertini, Phys. Rev. **137**, 1801 (1963); **188**, 1711 (1969).

[17]A. Bialas, Z. Phys. C **26**, 301 (1984).

[18]A. Capella, U. Sukhatme, and J. Tran Thanh Van, Z. Phys. C **3**, 329 (1980); A. B. Kaidalov, Pis'ma Zh. Eksp. Teor. Fiz. **32**, 494 (1980) [JETP Lett. **32**, 474 (1980)]; Yad. Fiz. **33**, 1369 (1981). [Sov. J. Nucl. Phys. **33**, 733 (1981)].

[19]S. Ritter and J. Ranft, Acta Phys. Pol. **B11**, 259 (1980); S. Ritter, Z. Phys. C **16**, 27 (1982); Comput. Phys. Commun. **31**, 393 (1984).

[20]K. Hänssgen and S. Ritter, Comput. Phys. Commun. **31**, 411 (1984).

[21]K. Hänssgen and J. Ranft, Nucl. Sci. Eng. **88**, 537 (1984).

[22]C. De Marzo *et al.*, Phys. Rev. D **26**, 1019 (1982).

[23]HELIOS Collaboration, A. Franz *et al.*, Nucl. Phys. **A447**, 475c (1986).

[24]W. Busza and A. S. Goldhaber, Phys. Lett. **139B**, 235 (1984); L. P. Csernai and J. I. Kapusta, Phys. Rev. D **29**, 2664 (1984).

[25]A. Capella, A. V. Ramallo, J. Tran Thanh Van, J. A. Casado, and C. Pajares, Z. Phys. C **33**, 541 (1987).